Supplementary Material

The impact of Holocene deglaciation and glacial dynamics on the landscape and geomorphology of Potter Peninsula, King George Island (Isla 25 Mayo), NW Antarctic Peninsula

Pablo A. Heredia Barión[1,2,3], Jorge A. Strelin[3,4], Stephen J. Roberts[5*], Cornelia Spiegel[2], Lukas Wacker[6], Samuel Niedermann[7], Michael J. Bentley[8], Emma J. Pearson[9], Nadia T. Manograsso Czalbowski[10,11], Sarah J. Davies[11], Bernhard Schnetger[12], Martin Grosjean[13], Stephanie Arcusa[13], Emma P. Hocking[14], Bianca Perren[5], Gerhard Kuhn[1,2]

[1]Alfred-Wegener-Institut Helmholtz-Zentrum für Polar- und Meeresforschung, Geosciences Division, Am Alten Hafen 26, 27568 Bremerhaven, Germany.

[2]University of Bremen, Department of Geosciences, Klagenfurter Str. 2-4, 28359 Bremen, Germany.

[3]Centro de Investigaciones en Ciencias de la Tierra (CONICET-UNC), Vélez Sársfield 1611, X5016GCA, Córdoba, Argentina.

[4]Instituto Antártico Argentino, Convenio MREC - Universidad Nacional de Córdoba, Vélez Sársfield 1611, X5016GCA, Córdoba, Argentina.

[5]British Antarctic Survey (BAS), Natural Environmental Research Council (NERC), High Cross, Madingley Road, Cambridge CB3 0ET, UK.

[6]ETH Zürich, Laboratory of Ion Beam Physics, Schafmattstr. 20, 8093 Zürich, Switzerland.

[7]Deutsches GeoForschungsZentrum GFZ, Telegrafenberg, 14473 Potsdam, Germany.

[8]Department of Geography, Durham University, Durham DH1 3LE, UK.

[9]School of Geography, Politics and Sociology, Newcastle University, Newcastle-upon-Tyne, NE1 7RU, UK.

[10]Instituto Antártico Argentino (I.A.A.), Av. 25 de Mayo. San Martín. Provincia de Buenos Aires (CP1650), Argentina.

[11]Aberystwyth University, Department of Geography and Earth Sciences, Aberystwyth, SY23 3DB, UK

[12]Institute for Chemistry and Biology of the Marine Environment (ICBM), Carl-von-Ossietzky-Str. 9-11, 26133 Oldenburg, Germany.

[13]Institute of Geography and Oeschger Centre for Climate Change Research, University of Bern, Switzerland.

[14]Department of Geography, Northumbria University, Ellison Building, Newcastle-upon-Tyne NE1 8ST, UK.

*** Corresponding author:** Stephen J. Roberts sjro@bas.ac.uk ORCiD: 0000-0003-3407-9127

This is a pre-print version of a paper published in Frontiers in Earth Science
https://doi.org/10.31223/X5606J
The final version may be different and will be available via the peer-reviewed publication doi link and in EarthArXiv https://eartharxiv.org/repository/view/4587/
We welcome all comments and feedback, posted on EarthArXiv or sent to the corresponding author, Stephen Roberts (sjro@bas.ac.uk).

1. Helium-3 cosmogenic nuclide surface-exposure dating

1.1 Sample processing

Four samples of 1 kg from basaltic boulders were used (Figure S1; see Table 3 for dimensions of erratics). To confirm the mineralogy and rock type of the samples, we made thin sections at CICTERRA, Córdoba, Argentina. The thin section analysis showed olivine and clinopyroxene phenocrysts, which represented 5-10 % of the total sample mass, with a modal grain size of ca. 200-500 µm. To process the samples, we used standard physical rock preparation (a jaw crusher, sieves (125 µm-1000 µm) and Frantz magnetic separation up to 1.5 A at Bremen University, Germany). As a first step, a slope on the machine of up to 24° and a low amperage (~0.10-0.20 A) was used to obtain magnetic grain separates from olivine and pyroxene, which represented the non-magnetic fraction. After that, we re-ran the non-magnetic fraction, this time at 0.20-0.30 A to concentrate the non-magnetic fraction. If feldspars remained, we ran the non-magnetic fraction using 1.5 A; pyroxene and olivine went to the magnetic side, feldspars to the non-magnetic side. Using di-iodomethane (DIM, $\rho = 3.3$ g cm^{-3}) we further concentrated the olivine and pyroxene separates. If the olivine and pyroxene separates still had any rock matrix attached, they were treated with dilute 5% HNO_3 followed by 30 minutes in an ultrasonic bath for cleaning. Masses were recorded before and after separation to track how much mass was lost. We examined purified pyroxene and olivine separates for each sample under a binocular microscope and back picked for further purity. Pyroxene dominated (99%) with only a minor amount of olivine. Four of the samples were analysed for cosmogenic He as one produced insufficient pyroxene and olivine.

1.2 He-3 preparation, methods, and analysis

The remaining steps of sample analyses were performed at the noble gas laboratory of GFZ Potsdam, Germany. Pyroxene separates were squeezed between two hard-metal plates in an ultra-high vacuum crusher to determine the trapped $^3He/^4He$. After crushing, pulverised samples were sieved to >100 µm before heating to minimise the contribution of atmospheric He irreversibly adsorbed to the grains (Protin et al., 2016). They were subsequently wrapped in Al foil and loaded to the sample carousel above the resistance-heated extraction furnace, which was baked at 100°C for one week. Noble gases were extracted in two heating steps at 900 and 1750°C (with an initial 600°C step for sample 02-Potter), purified in two Ti sponge and foil getters and two SAES (ZrAl) getters, and measured in a Helix SFT mass spectrometer using procedures similar to Niedermann et al. (1997). ^4He blank values were (2-10) × 10^{-12} cm^3 STP for crushing extractions, (4-5) × 10^{-12} cm^3 STP for 600 and 900°C heating steps and (18-40) × 10^{-12} cm^3 STP for 1750°C steps. Helium concentrations were calculated by peak-height comparison with our in-house noble gas standard, an artificial mixture of the five noble gases in nitrogen with a $^3He/^4He$ ratio of (21.66 ± 0.24) × 10^{-6} (Blard et al., 2008, 2015). Two aliquots of the CRONUS-P pyroxene standard material were measured alongside the samples and gave ^3He concentrations of 4.86 ± 0.10 × 10^9 and 4.79 ± 0.10 × 10^9 at g^{-1}, which agree within 2σ uncertainties with the global mean value of 5.02 ± 0.12 × 10^9 at g^{-1} (Blard et al., 2015).

1.3 Calculations of exposure ages and results

We used a rock density of 2.7 g cm^{-3}. No correction for erosion was included in the age calculations because we did not find clear evidence of substantial erosion. Shielding by snow accumulation on the boulders was not included but could be a substantial factor influencing exposure ages from Potter Peninsula. Snow accumulates up to 10 cm in Potter Peninsula, and between 2 and 5 cm on the top of hummocky areas (Winkler, 2000). However, strong winds remove accumulated snow on the top of hummocks, so it is preserved for no longer than 50 days per year (Wunderle et al., 1998; Winkler, 2000). Moreover, rainfall occurring both in summer and winter periods also contributes to only a short period of snow cover (Falk and Sala, 2015). We assumed that past snow accumulation on the Potter Peninsula is insignificant on top of morainic crests of the Three Brothers Hill moraine system with respect to the long-term integrated exposure history.

To calculate ^3He exposure ages, the ^3He concentrations specifically produced by cosmic ray irradiation ($^3He_{cosmo}$) were determined. Ideally, He in phenocrysts is a mixture of only magmatic and cosmogenic

components. If so, the concentration of cosmogenic ^{3}He is calculated using the following equation (Niedermann, 2002):

$$^3He_{cosmo} = {}^4He_{heat} \times (^3He/^4He_{heat} - {}^3He/^4He_{crush})$$

$^4He_{heat}$ is the ^{4}He concentration and $^3He/^4He_{heat}$ the isotope ratio determined during stepwise heating, while $^3He/^4He_{crush}$ is the isotope ratio determined by crushing the mineral separates in vacuo. The latter method selectively releases gases trapped in fluid and melt inclusions. In contrast, heating also releases gases from the crystal lattice, such as cosmogenic He. The cosmogenic component is calculated by subtracting trapped ^{3}He from the total ^{3}He that is released by heating of the sample powders in vacuo. However, in our samples $^3He/^4He_{crush}$ ratios were systematically higher than $^3He/^4He_{heat}$; hence, exposure ages calculated according to the equation above are negative. This is because in old basalts such as those analysed here, radiogenic ^{4}He produced by decay of U and Th (either in the phenocrysts or implanted from the basalt matrix; Williams et al., 2005) and ^{3}He generated by the thermal neutron capture reaction $^6Li(n, \alpha)^3H \rightarrow {}^3He$ (Dunai et al., 2007) may be present as well. Indeed, the $^3He/^4He_{crush}$ values were lower than expected for typical magmatic He (Table 4, indicating that radiogenic He dominates over magmatic He and is even extracted by crushing. Therefore, instead of using $^3He/^4He_{crush}$ in the equation above, we assumed that magmatic He is negligible and thus non-cosmogenic He is essentially represented by radiogenic He with a typical $^3He/^4He$ ratio of 0.028×10^{-6} (0.02 Ra, where Ra is the atmospheric $^3He/^4He$ ratio). To be conservative, a 100% uncertainty was assigned to that value. Because of the dominance of radiogenic He, which prevented a determination of the magmatic $^3He/^4He$ ratio as some radiogenic He was even released by crushing, a mere correction for radiogenic ^{4}He based on U and Th contents (Blard and Farley, 2008) is not feasible for these samples.

2. Stratigraphic sediments: grain size analysis

Thirteen samples were dry sieved to separate the fraction larger than 2 mm, placed in an ultrasonic bath for 10 seconds, then placed in a reciprocating shaker and left overnight. Samples were wet sieved to separate the fraction <0.063 mm (silt and clay size), and the coarser fraction was dried in an oven at 50ºC and dry sieved into sand fractions (>1mm, >0.5 mm, >0.25 mm, >0.125 mm and >0.063 mm). The silt and clay fractions were transferred to a sedimentation cylinder and fine and coarse silt separated from clays after settling using the pipette method. The clay fraction was then concentrated using a centrifuge, and all fractions were dried in an oven at 40ºC.

3. Lake sediments

3.1 Supplementary Site Descriptions (all names used in this section are informal)

Potter Peninsula Lakes: Following an initial two-day survey of the area and lakes L0-L2, L4-L8, L14-L19 (Figure S2) that revealed that most of the lakes in the Carlini Station area to be gravel bottomed and unsuitable for coring, we decided to work on Lake L5 (Matias Lake), which was half frozen towards Lake L6 (Rudy Lake), but its deepest point close to base of Three Brothers Hill was covered by ~1 m thick ice, providing a stable platform for coring. Lake L7 was half ice-covered, with an ice-free moat around the edge and therefore not safe to work on. L4 and L13 turned out to be snow-covered shallow meltwater ponds. The ice on Lake L6 (Rudy Lake) and parts of Lake L8 (Superior Lake) appeared transparent in large sections and constructed of unstable candle ice. Given the size of Lakes L6 and L8 and the potential distance of the central and deepest points from safety, we decided to work on smaller, more accessible basins. Lake L15 (GPS Lake) is a small bedrock-formed basin, which was partially ice-free when we arrived at Carlini Station in early November 2011, but later refroze while coring Lake L5. Lakes L3, L10-13 and L24-30 were visited and preliminary limnological measurements made for future potential visits on a two-day trip at the end of the field season (mid-December 2011). We collected penguin samples from around the lake behind Refugio Elefante – Lakes L11, L12, L24, L25 and L25a. Lake L11 has a sill height of <10 m a.s.l., below the Holocene marine limit of 16 m a.s.l., and of interest for future isolation basin/RSL studies. Lake L11 was ice-free when we arrived, so an early spring (September-October) trip and/or earlier field season input

would be needed to core from a stable ice-covered platform. Colleagues from Uruguay attempted to core water/dinghies later in the season. They collected 5-6 cm of glacially derived sediments but found it difficult to core deeper from a dinghy-based raft. When frozen, Lakes L11, L12, L24 and L25 would make good study sites for assessing the influence that penguins have on lakes sediment processes and possibly provide a palaeo-guano based history of penguin colonisation (cf. Roberts et al., 2017). Lakes L31 and L32 were not visited but could provide interesting sites for modern process and/or constraints on recent deglaciation/readvance on the SW Warszawa Icefield.

Matias Lake (Lake L5: *62 14'42.0714S, 58 39'52.164W):* Matias Lake is a shallow (<6 m deep) bedrock basin formed within 'Neoglacial' moraines on between Three Brothers Hill and the Warszawa Ice Cap on Potter Peninsula (del Valle et al., 2004). In the Austral winter, Matias Lake and Lago Rudy form separate basins. During the austral spring/summer, as water levels rises, a single lake is formed around the small moraine hummock at its eastern end. After Lago Superior (L8 Superior Lake; Figure S2), the Lago Rudy/Matias Lake basin is the second largest permanent water body on Potter Peninsula. Lago Rudy is surrounded by elevated palaeo-lake terraces ~7.4 m and 3.6 m above the lake level (measured by dGPS; del Valle et al., 2004). Del Valle et al. (2004) extracted a ~145 cm long core from the deepest point (c. 6 m) at the eastern end of Matias Lake, near the base of a steep scree slope on the western side of Three Brothers Hill using a wide-bore piston corer that could penetrate the basal diamicton unit.

Thirteen cores and water samples were taken from MAT1-7, including from two smaller basins located away from the influence of the scree slope. We also took five surface cores along a longitudinal transect (ST0–ST4) on the central GPR Line 16 from the deepest point of the lake towards the shallow Rudy Lake inflow (Figure S3). The Livingston corer was the most successful of the coring equipment used. Nevertheless, we were not able to penetrate through a layer of gravel at c. 20-30 cm depth, despite numerous attempts. No sub-aquatic moss was retrieved from the surface of the lake.

Lake L15 (62 14'26.016S, 58 40' 39.468W): Lake L15 (GPS Lake) is a shallow (<2 m deep) bedrock basin with a retaining sill at ~20 m a.s.l. located on the western tip of Potter Peninsula (Table S4), immediately south of the western lighthouse and adjacent to the Trimble GPS (bedrock-fixed) triangulation station and a small red hut containing GPS receiving equipment. Lake L15 is the furthest permanent body of water from the Warszawa Icefield on Potter Peninsula and has three outflows, two of which are active and one which is elevated and detached from the present lake (Figure S2B). No marine sediments have been found in lakes below 16 m on Potter Peninsula, and cores extracted from Lake L15 are a freshwater record that can be used to constrain the timing of past glacial advance/retreat. Lake L15 had one snow patch and meltwater inflow stream, which was covered in moss and ~1–2 m higher than the ice level on the lake at the time of coring. Lake L15 was partially ice-covered at the time of coring with ~1 m thick ice covering the eastern side of the lake. Although thick enough to stand on initially, the thin ice-cover melted quite rapidly and was no longer a stable and safe platform for coring.

3.2 Supplementary Methods

Surveying: At Lake L5, we undertook a GPR survey on the lake ice using a Reflex system with Leica dGPS attached. Measurements were taken every 10 seconds across an approximately N-S and E-W oriented grid (Figure S3). Suitable coring sites in flat-bottomed basins and the depocentre of the lake (MAT1) were identified from on-site preliminary processing of GPR data. The location of the depocentre determined in our GPR survey matched that of del Valle et al (2004). As Lake L15 was partially ice-free when cored, we measured the geoid-corrected elevation above sea level (m a.s.l.) of the lake surface and its inflows/outflows using a Trimble differential GPS (dGPS), with a precision of 0.1 m or better (Table S4).

Limnology: Vertical profiles of lake water conductivity, temperature and oxygen saturation using YSI MDS 600 water quality metre at 10 cm intervals from the deepest point in Matias Lake and Lake L15. Limnological and water chemistry data are shown in Figure S4 and Tables S5, S6. Water samples for additional analysis were collected in acid-washed Nalgene bottles and filtering the water for pigments using a UWITEC water sampler. Zooplankton and phytoplankton samples were taken plankton nets and Whatman GF/C filters respectively (preservation in ethanol).

^{210}Pb and ^{137}Cs dating: Approximately 4 g of crushed and dried sediment was added into tubes to a predefined level and sealed gas tight. After at least 21 days of storage to obtain radioactive equilibrium between ^{226}Ra and ^{222}Rn, activities of radionuclides were measured by well-type gamma spectrometry (Ge-detector, GWC 2522-7500 SL, Canberra Industries Inc., USA) and processed with GENIE 2000 3.0 (Canberra Industries Inc., USA). The following nuclides and energies were used for quantification: ^{210}Pb excess = ^{210}Pb: 46.5 keV – (mean of ^{214}Pb: 351 keV + ^{214}Bi: 609 keV), ^{241}Am: 59.5 keV and ^{137}Cs: 661 keV. Counting statistics for ^{210}Pb, ^{214}Pb and ^{241}Bi were better than 5% and for ^{137}Cs < 15% except for samples lower than 5 cm sediment depth. ^{241}Am could not be detected. Trueness of this method was tested by using the standard reference materials UREM-11 (^{210}Pb, ^{214}Pb, ^{214}Bi), IAEA-384 (^{241}Am, decay corrected), and IAEA-385 (^{241}Am, ^{137}Cs, decay corrected). To take account of changing sedimentation rates with time, the age of each sediment slice was determined according to the constant rate of supply model (CRS) after Appleby and Oldfield (1978). Compaction effects were considered by correcting the radiolead excess activities with the dry bulk density. The total ^{210}Pb inventory was determined by integration of the excess ^{210}Pb activity data versus the depth profile. Mass accumulation rates of the bulk sediment were calculated from the product of the sedimentation rate and the dry bulk density.

Catchment sampling: Catchment samples were taken from around both lakes (Figure S2, S3). We also surveyed 10 areas (P1-P10; Figure S3B, E) where stable moss banks and cyanobacterial mats had formed. Moss development on Potter Peninsula was limited to the area furthest from the glacier front around Lake L15 and on the exposed northern slopes of Three Brothers Hill. Short cores, ~6-18 cm in length, were taken from thickest moss banks in three sampling areas: P1, P2, P5 in the L15 catchment area (Figure S2B). Sample areas P1-2 and P7-9 are waterlogged moss banks ~18-20 m a.s.l. surrounding small, shallow ponds formed from snowbank melt (P1) and/or the outflow of L15 (P2 and P9). Well-developed microbial (cyanobacteria) mats up to 10-12 cm thick were also found at P2, fed mainly by snowmelt from the slopes of Three Brothers Hill. Moss bank P3 is located above Lake L15 and snowmelt from it feeds into the lake. Sample area P4 is a small area of thinly developed moss and P5 is a relatively well-developed, dry 'carpet' moss bank on a raised ridge at ~ 40 m a.s.l.

3.3 Supplementary Results

Surveying: Based on corrected mean Trimble dGPS elevation data (one hour measurement time), the mean ellipsoid height of five locations (four outflows and one inflow) for Lake L15 was 42–43 m. Since the ellipsoid correction factor is 21.48 m at this location, the altitude of Lake L15 is ~21 m.

Limnology: Both lakes had maximum water profile temperature of between 1-1.5°C, low conductivity and dissolved oxygen between 20-80%, reducing with depth in the water column. The depocentre of Matias Lake is ice-covered for at least nine months of the year, and in shadow from ~3 pm onwards in mid-summer. Poor light penetration and persistently low lake water temperature have created unfavourable conditions for moss growth. In contrast, surface moss was retrieved from the shallower and partially ice-free Lake L15 (and all lakes cored on Fildes Peninsula by Watcham et al., 2011). While coring at Lake L15 in late November, the water in the western side of the lake often refroze with daytime temperatures of -5 to 1°C and night temperatures down to -8°C.

^{210}Pb and ^{137}Cs dating: The ^{210}Pb CRS age model and ^{137}Cs data from the Matias Lake MAT1 record show good agreement (within ±5 years), with the c. 1962 CE bomb-testing peak in ^{137}Cs having a c. 1964 CE ^{210}Pb CRS age. ^{241}Am is below detection limits in both records. The ^{137}Cs record likely starts at c. 1935 CE due to downward mobility in this element. An association with the 1986 Chernobyl reactor explosion is unlikely to be the cause of the small ^{137}Cs at c. 1989 CE, but this cannot be completely ruled out. The uppermost 10 cm have a sedimentation rate of ~1 mm yr^{-1}. The increase in the sediment accumulation rate from c. 1960 CE onwards is likely due to increased melt as the Fourcade Glacier retreated from its 1956 CE limits (Fig. 2). For Lake L15, results from the ^{210}Pb Constant Rate of Supply (CRS) age model show the sedimentation rate in the top 10 cm is ~0.3–0.5 mm yr^{-1} with the sample at ~4-5 cm at least 150 years old. The ^{210}Pb data are consistent with radiocarbon ages that show sediment between 6 and 6.5 cm is 620±80 a cal BP, Sediments at 3–3.5 cm and 0–0.5 cm depth were deposited in the 'post-bomb'/ modern era, most

likely between -40 – -44 cal yr BP (1990–1994 CE) (Fig. S4; Table 2). ^{137}Cs data are not consistent with the ^{210}Pb CRS age model, and it is possible that the steep increase in ^{137}Cs in the upper 2 cm relates to a ^{137}Cs 'soil reservoir', leaching ^{137}Cs into the lake from snow or lake-ice melting rather than direct deposition from the atmosphere. As the prerequisite for the CRS model is not fulfilled because the flux of ^{210}Pb has changed through time and is not constant, we do not show an age-depth model for this record. Pb-210 flux can increase, for example, when released by a melting glacier, leading to enhanced emission of Rn and a higher sedimentation of ^{210}Pb compared to ^{137}Cs. Further investigation of these effects in Antarctic lacustrine environments is recommended.

4. Radiocarbon dating

4.1 Additional methods for carbonate samples

Typically, 1 mg of carbonate was analysed at ETH Zurich by first leaching samples with 100 µl 0.02 M HCl to remove any surface contamination, before the remaining the carbonate was dissolved in 100 µl 85% phosphoric acid in 4.5 ml septa sealed vials. The CO_2 formed in the leach fraction was only measured for quality control. No strong surface contamination was measured for any samples used in this study. Consequently, we only report the results from the CO_2 of the main fraction that was measured with a gas interface coupled to a MICADAS type AMS system (Wacker et al., 2013; Bard et al., 2015).

4.2 Marine reservoir ages for the South Shetland Island and the Antarctic Peninsula

Heaton et al. (2020, 2022) highlighted the general unsuitability of marine calibration curves in the Polar Regions. Non-constant, and large, age offsets exist, particularly for samples from Last Glacial Maximum and colder stadials due to increased surface-ocean marine depletion of ^{14}C caused by localised changes in ocean circulation, local sea-ice cover, and wind stress.

The total radiocarbon marine reservoir age (MRA) is made up of two components, the global average MRA (R) and local MRA (ΔR), where ΔR is defined the offset from the global surface-ocean average age i.e., MR = R + ΔR (Hall et al., 2010). The local MRA (ΔR) is generally larger in the Polar Regions, and it varies in time and due to localised changes in oceanographic parameters (e.g., sea ice cover, upwelling, wind stress) (Hall et al., 2010; Ó Cofaigh et al., 2014; Heaton et al., 2020). The selection of a suitable ΔR value needs to take these factors into account, but, as highlighted by Hall et al. (2010), ΔR values have been inconsistently (and sometimes incorrectly) applied in Antarctic studies. ΔR values often reflect the closest and/or most biologically and oceanographically suitable ΔR value for a specific location (e.g., Emslie, 1995; Watcham et al., 2011; Roberts et al., 2017), an Antarctic-wide value based on paired ages from one location (e.g., Hall et al., 2010), or a community-agreed value (e.g., Ó Cofaigh et al., 2014).

The issue of spatial and temporal variability in ΔR in Antarctica was addressed by Hall et al. (2010) who compared paired radiocarbon and U/Th ages from corals in the Ross Sea region. The average MRA of 1144±121 ^{14}C years and ΔR value of 791±121 ^{14}C years for the last 6,000 years was recommended as a starting point for assessing ΔR values and this value was used by Hall (2010) on the South Shetland Islands (SSI). The causes and impact of temporal variations in ΔR in and around Antarctica were discussed further by Ó Cofaigh et al. (2014). The main advantage of the Marine20 calibration over its predecessors is that it accounts for one of the two main sources of error affecting all marine radiocarbon ages, i.e., temporal variations in the global MRA. Variations in the global MRA are comparatively minor during the Holocene in Marine20, but they are ~150 ^{14}C years larger than Marine13, meaning all previous ΔR values need to be recalculated.

South Shetland Islands ΔR: Published local marine reservoir ages (ΔR) for the SSI range between ~600 and 1,300 years (e.g., Curl, 1980; Björck et al., 1991; Gordon and Harkness, 1992; Berkman and Forman, 1996; Milliken et al., 2009; Hall et al., 2010; Hass et al., 2010; Watcham et al., 2011), and are generally lower than values ΔR for the Antarctic Peninsula (AP), Signy Island and Weddell Sea. Hall et al. (2010) used a

ΔR of 791 ± 121 ^{14}C years based on paired radiocarbon and uranium–thorium dates from Antarctic solitary corals. This was supported by results of Simms et al. (2012), who used OSL of cobble surfaces to investigate the depositional age of beach ridges on KGI. The lowest ΔR value of 664±10 ^{14}C years in Watcham et al (2011) was based on the average ^{14}C age of surface waters around the SSI of 1,064±10 ^{14}C years, measured by Wellner et al. (pers. comm. in Watcham et al. (2011), calculated, in 2010, as ΔR = 1064 - 400 ^{14}C years). These samples were collected after 1950 CE and could have a similar pre- and post-bomb ages offsets of up to c. 500 years, similar to pre- and post-bomb samples dated by Berkman and Forman (1996).

A ΔR value of 700±100 ^{14}C years proposed by Emslie (1995) has been commonly applied to radiocarbon ages obtained from penguin bones, feathers, and guano-influenced deposits from the SSI (Emslie, 2001; Emslie et al., 2013; Roberts et al., 2017; Emslie et al., 2019). This values was based on an assessment of ΔR values from the Ross Sea, coupled with nearby ΔR values in Björck et al. (1991) of 829±50 ^{14}C years (location no. 523 in the Marine13 online database, but originally ΔR=805±50 ^{14}C years in Emslie (1995)) from Adelie penguins collected prior to 1950 CE (1903 CE) from Hope Bay (radiocarbon ages of 1280±50 ^{14}C years; located across the Bransfield Strait from the SSI), and a ΔR value of 640±60 ^{14}C years (not in the Marine 13/20 online database) based on radiocarbon ages 1040±60 ^{14}C years from a gentoo penguin collected from South Georgia in 1913 CE. Emslie (2001) concluded that the similarity between radiocarbon ages calibrated with this and other ΔR values of 750±50 and 800±50 ^{14}C years meant local corrections for variable upwelling and/or changes in sea-ice cover during the Holocene through time might not be necessary. Emslie (1995) argued that the ΔR value should be smaller than that from the Ross Sea area, where more upwelling of older carbon from depth occurred, but younger than the South Georgia ΔR value, where less upwelling existed. The recalculated Marine20 ΔR value for the Björck et al. (1991) ΔR value is 669±50 ^{14}C years, ~160 ^{14}C years less than its equivalent Marine13 ΔR value.

The Calib online databases provide a consistent, open and transparent calculation method for ΔR values, and is backwards and forwards compatible across all calibration curves. Individual or combined weighted mean regional ΔR values closet to the SSI were extracted and calculated using tools within the Marine20 online database and compared similarly obtained data from the Marine13 online database (Table S7). A number of different values ΔR for the AP exist, but there are currently only three data entries from three locations in the Marine13 and Marine20 online databases (http://calib.org/marine/ and http://calib.org/marine13/) (entries 521, 522, 523 in Table S7). This increases to six entries from four locations if Signy Island is included (entries 516, 517, 518, 521, 522, 523 in Table S7). There are no ΔR values in the Marine13/20 databases from the SSI or South Georgia, and no detailed investigations comparing paired radiocarbon and U/Th (or other radiometric) ages similar to Hall et al. (2010) have been undertaken for the AP region.

After assessing published ΔR values, we concluded that for consistency and more transparent compatibility between calibration curves, the most suitable ΔR value to for the SSI should be based on the closest and most biologically and oceanographically suitable values in the Marine13 and Marine20 online Calib database. The new Marine20 ΔR value for the SSI of 666±76 ^{14}C years used in this study represents the weighted mean ΔR value for the northern Antarctica Peninsula (NAP) and Signy Island (Table S7). This ΔR value is statistically indistinguishable from the recalculated Marine20 ΔR value of 669±50 ^{14}C years for the closest radiocarbon dated marine sample collected prior to 1950 from Hope Bay (location 523 in the Marine20 online database; previously ΔR=829±50 in Marine13) (Björck, 1991) as well as a newly recalculated Marine20 weighted mean ΔR value from Signy Island of 665±91 ^{14}C years (Table S7). ΔR values from the NAP and Signy Island were combined since brachiopods source and assimilate carbon in a similar manner to the bivalves dated in this study. Our rationale for using a regionally weighted mean ΔR value for areas with similar mixing and upwelling of 'old' water is the same as Emslie (1995), and aligns with the 'smaller' local marine reservoir corrections used by previous studies from the SSI (Watcham et al., 2011; Simms et al., 2012).

Antarctic Peninsula ΔR: Previous data compilation papers recommended using a ΔR value of 830±100 ^{14}C years for the AP (Ó Cofaigh et al., 2014). This was based on a total MRA of 1230±100 ^{14}C years but does

not relate to any ΔR values (or combination of ΔR values) from the AP region in the Marine13 and Marine20 databases making it difficult to recalculate. Derived from Domack and Ishman (1992), the Ó Cofaigh et al. (2014) recommended value is similar to the Björck et al. (1991) Marine13 ΔR value of 829±50 ^{14}C years. The Björck et al. (1991) ΔR value represents -451 ^{14}C years from the total MRA of 1280±50 ^{14}C years in Marine13, rather than -400 ^{14}C-year in Ó Cofaigh et al. (2014), reflecting between the Marine09 and Marine 13 calibration curves. Despite these discrepancies, the Ó Cofaigh et al. (2014) ΔR value is essentially the same as the Björck et al. (1991) ΔR value in Marine13, albeit with an additional +50 ^{14}C year error.

Overall, we found that there were no statistically significant differences between Holocene radiocarbon ages calibrated using the SHCal13 (Hogg et al., 2013) and Marine13 (Reimer et al., 2013) and the ShCal20 (Hogg et al., 2020) and Marine20 (Heaton et al., 2020) curves (ShCal13 vs 20: n=19, mean difference ± 1σ = -4±8 years; Marine: n=8, mean difference ± 1σ = -45±8 years). Comparisons between calibrated SHCal13 and Marine13 ages therefore remain valid. However, southern and northern AP sites have statistically different ΔR values of 844±42 and 666±76 ^{14}C years in the Marine20 database (Table S7). Simms et al. (2021) recalculated the Hall et al. (2010) 'pre-1950' surface radiocarbon age data in the Marine20 database and used this ΔR for the NAP. We considered using this or updating the Hall et al. (2010) Holocene average ΔR value of 791±121 ^{14}C years to Marine20 as the latter has been used in several papers for the SSI. Ultimately, we decided not to because both these values represent conditions in the Ross Sea region, which is ~4,000 km from the SSI, and are unrelated to ΔR values from the NAP. Nevertheless, the recalculated Marine20 ΔR value of 641±121 ^{14}C years for the Hall et al., (2010) ΔR value of 791±121 ^{14}C years is similar and overlaps with the recalculated Marine20 weighted mean ΔR value of 666±76 ^{14}C years for the NAP and Signy Island used in this study.

5. Data availability

Datasets can be obtained from the NERC EDS UK Polar Data Centre (PDC) as follows:

Bentley, M., Roberts, S., Heredia Barión, P., Strelin, J., Spiegel, C., Niedermann, S., & Wacker, L. (2022). Chronological and sedimentological data from Potter Peninsula, South Shetland Islands. (Version 1.0) [Data set]. NERC EDS UK Polar Data Centre. https://doi.org/10.5285/4671A42F-7A2E-4883-948C-EF6B26DD41C9

Roberts, S., Pearson, E., Czalbowski, T., Davies, S., Grosjean, M., Arcusa, S., & Perren, B. (2022). Chronological, geochemical and sedimentological data from a lake sediment record extracted from Lake L5 (Matias Lake) on Potter Peninsula, South Shetland Islands in 2011. (Version 1.0) [Data set]. NERC EDS UK Polar Data Centre. https://doi.org/10.5285/6575CD7A-CFBA-4820-9FA6-257161B4D24B

Roberts, S., Pearson, E., Czalbowski, T., Davies, S., Grosjean, M., Arcusa, S., & Perren, B. (2022). Chronological, geochemical and sedimentological data from a lake sediment record extracted from Lake L15 (GPS Lake) on Potter Peninsula, South Shetland Islands in 2011 (Version 1.0) [Data set]. NERC EDS UK Polar Data Centre. https://doi.org/10.5285/2031310D-1E35-4EA1-A1CC-CD318E82D394

Roberts, S., Hocking, E., & Heredia Barión, P. (2022). Compilations of new and published age data constraining glacier advance, retreat and aquatic moss layers in lakes from the South Shetland Islands (Version 1.0) [Data set]. NERC EDS UK Polar Data Centre. https://doi.org/10.5285/9337F8F4-1A8F-4156-8F79-7A249F733117

All code, data, packages and package references, are also available on Github. Further inquiries and requests should be made to the corresponding author. The satellite images used in this paper and its Supplementary Material are Maxar products © 2022 Maxar technologies and have been reproduced at low resolution under license to BAS.

6. Figures & Tables

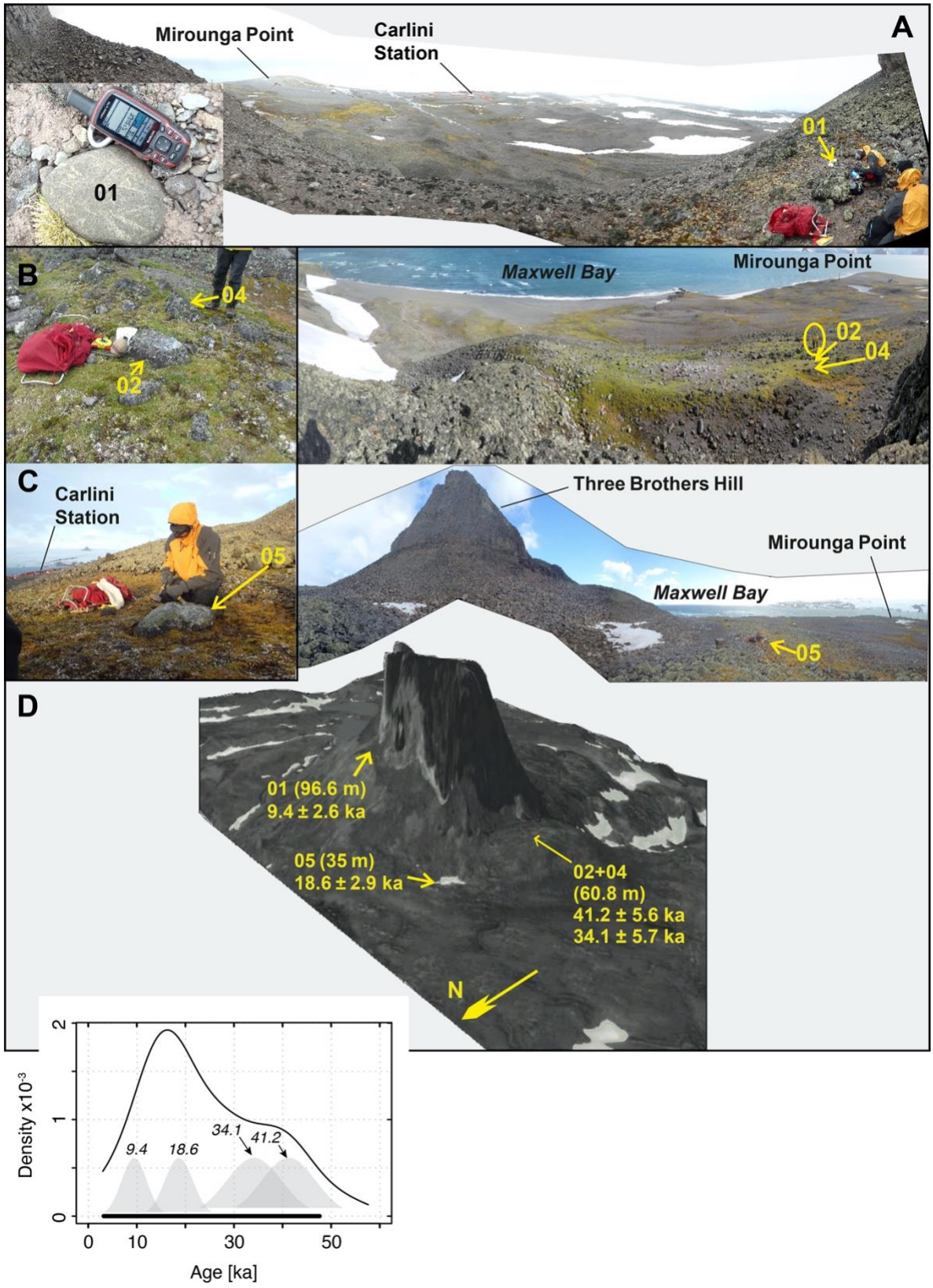

Figure S1. Field pictures of the dated glacial erratic samples on marginal moraines around Three Brothers Hill. A) Sample 01-Potter; B) Samples 02- and 04-Potter; C) Sample 05-Potter; D) Digital Elevation Model of Three Brothers Hill showing the positions of all samples with their ^{3}He exposure ages and age probability density distributions and phases (black bars) (at 95% confidence).

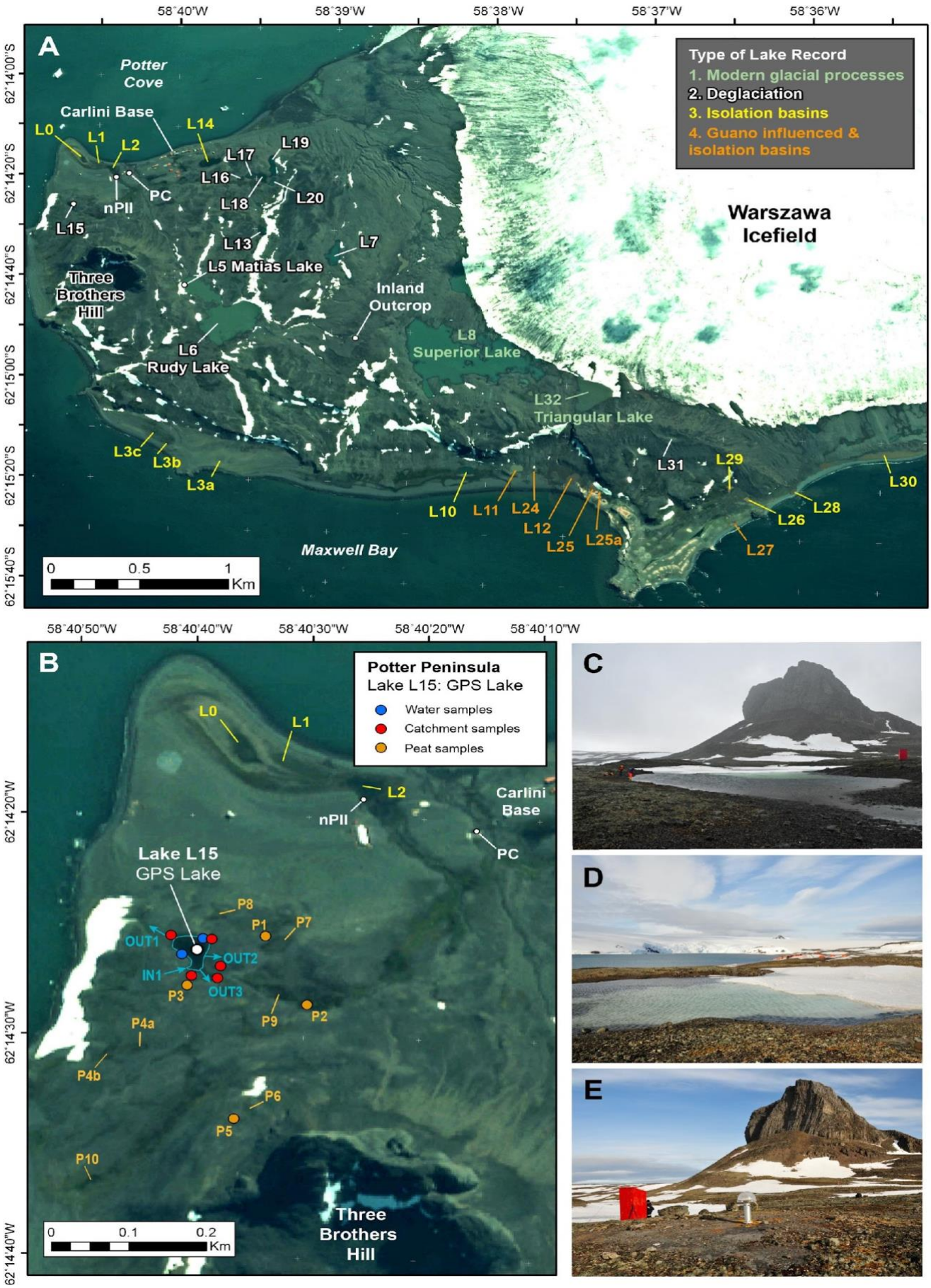

Figure S2. A) Lakes on Potter Peninsula, classified according to type of record and their relationship to the landsystem assemblages described in the main text. B) Close up of Lake L15 showing coring locations and

sampling sites around the lake. C) Partially ice-free L15 (GPS Lake) taken on 13/11/11 looking ~SE towards Tres Hermanos (Three Brothers) Hill and the red GPS hut. D) View of partially ice-covered Lake L15 looking ~NE towards the Fourcade Glacier at the head of Potter Cove; E) View of the dGPS triangulation station and GPS hut on the shore of Lake L15. The background satellite image in (A) and (B) is scene ID: 1010010004C1B200; pixel resolution .67 m; Maxar Products. Quickbird satellite image acquired 16/01/2006 © 2022 Maxar technologies.

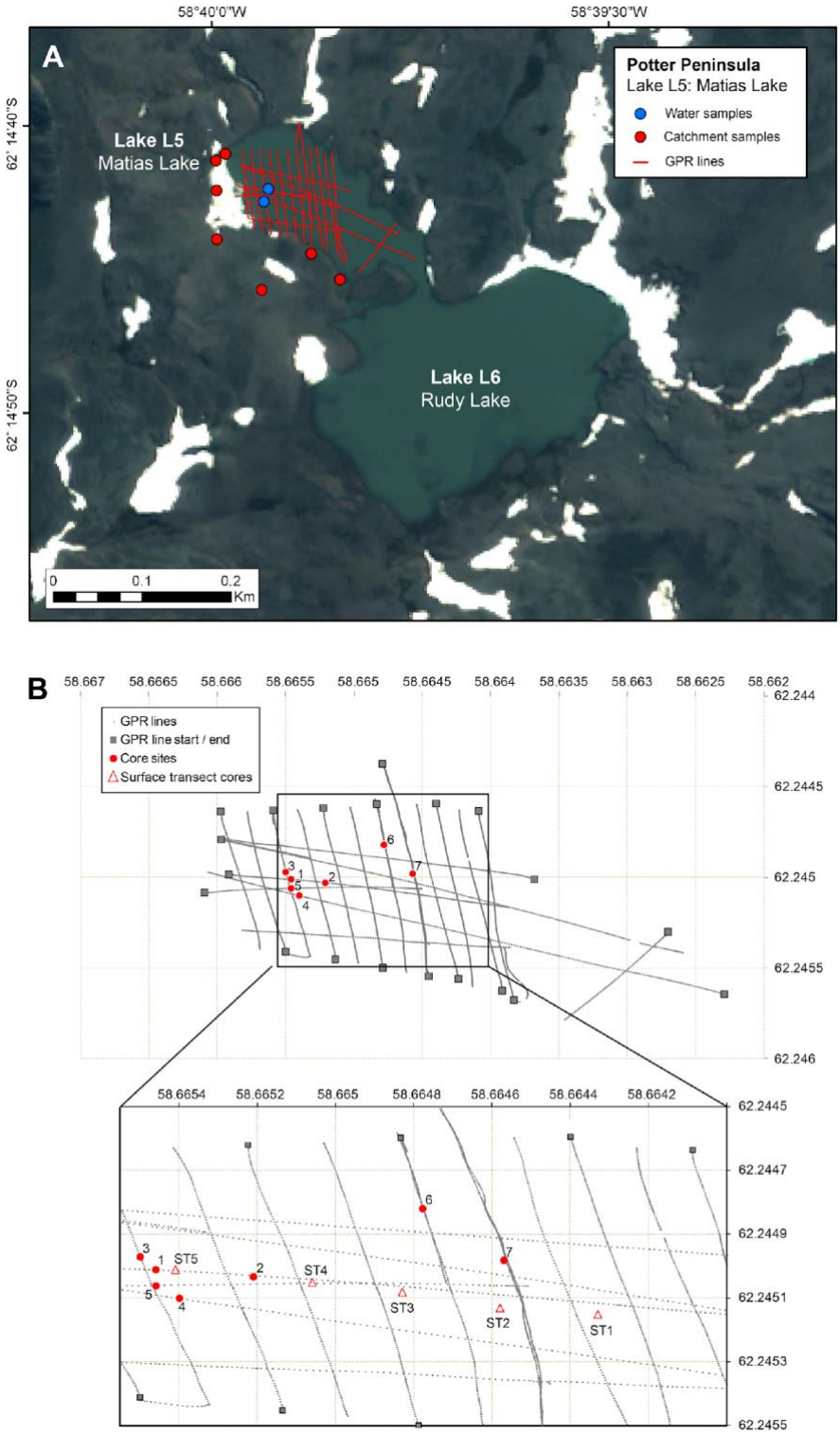

Figure S3. A) Sampling and Ground Penetrating Radar (GPR) survey lines on Lake L5 (Matias Lake). B) GPR survey lines and coring locations on Lake L5 (Matias Lake). The background satellite image in (A) and is scene ID: 1010010004C1B200; pixel resolution .67 m; Maxar Products. Quickbird satellite image acquired 16/01/2006 © 2022 Maxar technologies.

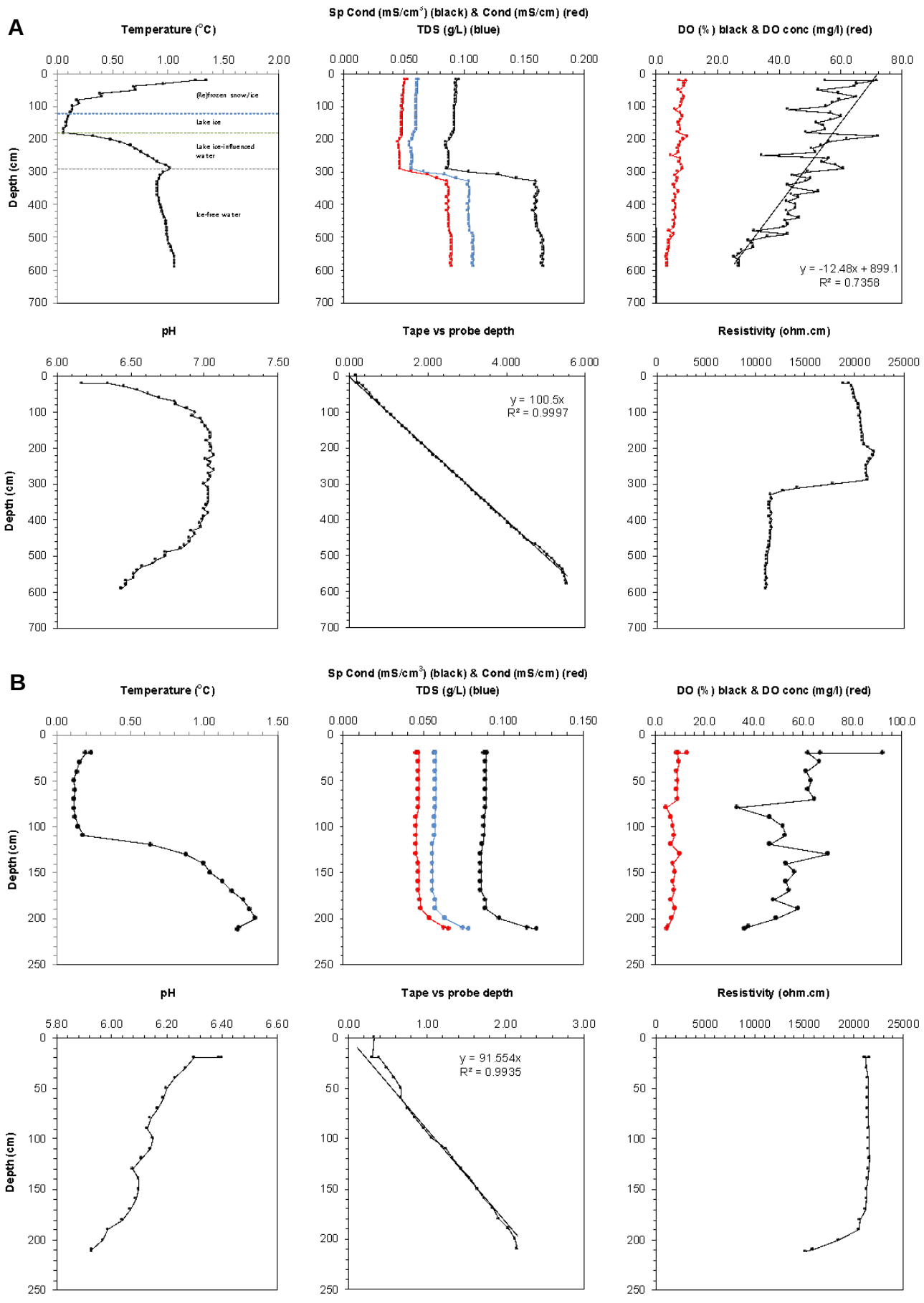

Figure S4. Limnological properties of A) Lake L5 (Matias Lake) and B) Lake L15 (GPS Lake).

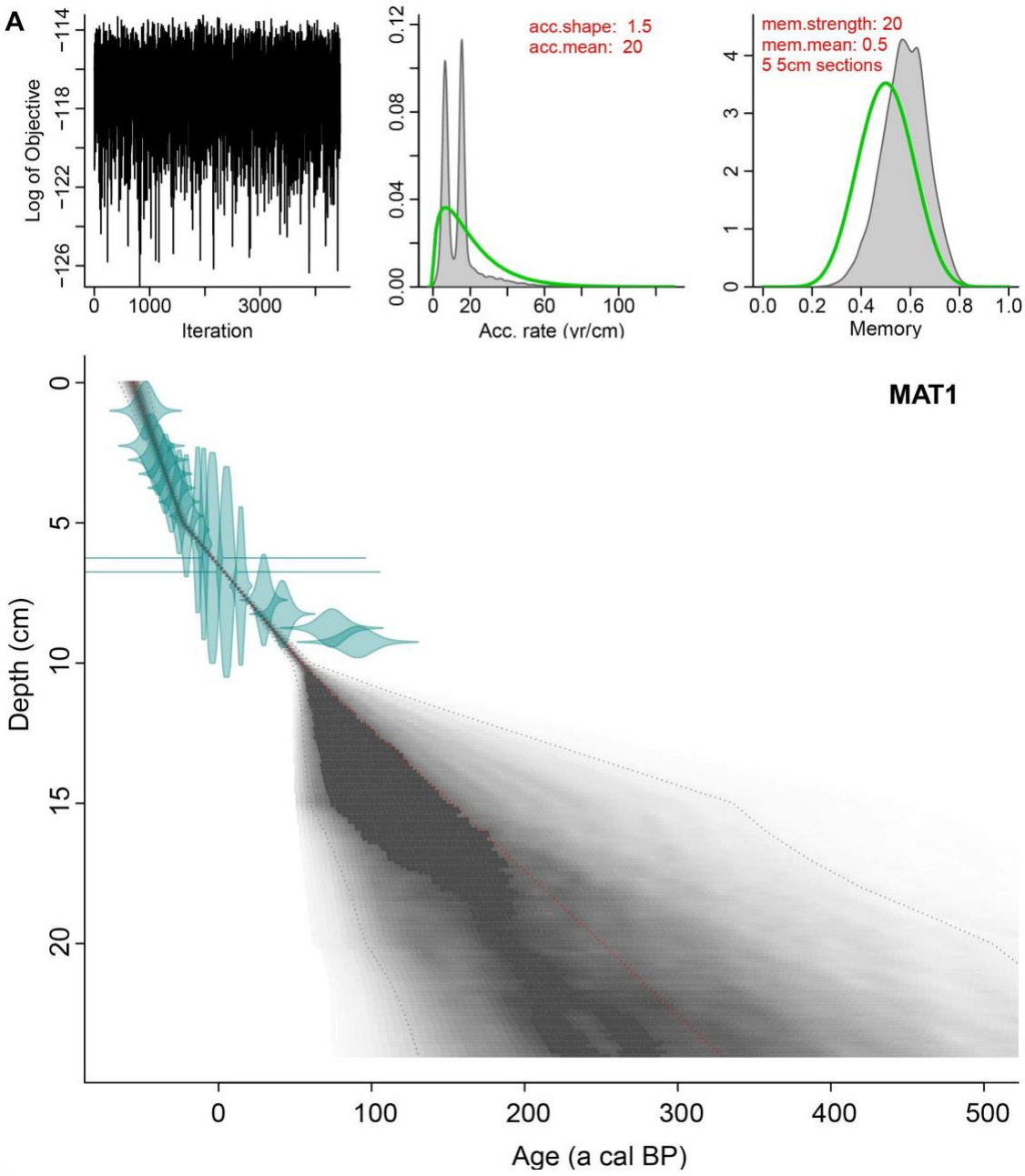

Figure S5. Bayesian age-depth model for Matias Lake (L5)

Figure S6. Aquatic moss extracted from Lake L15 Unit 3 (uppermost 6.5 cm) which was used for radiocarbon dating.

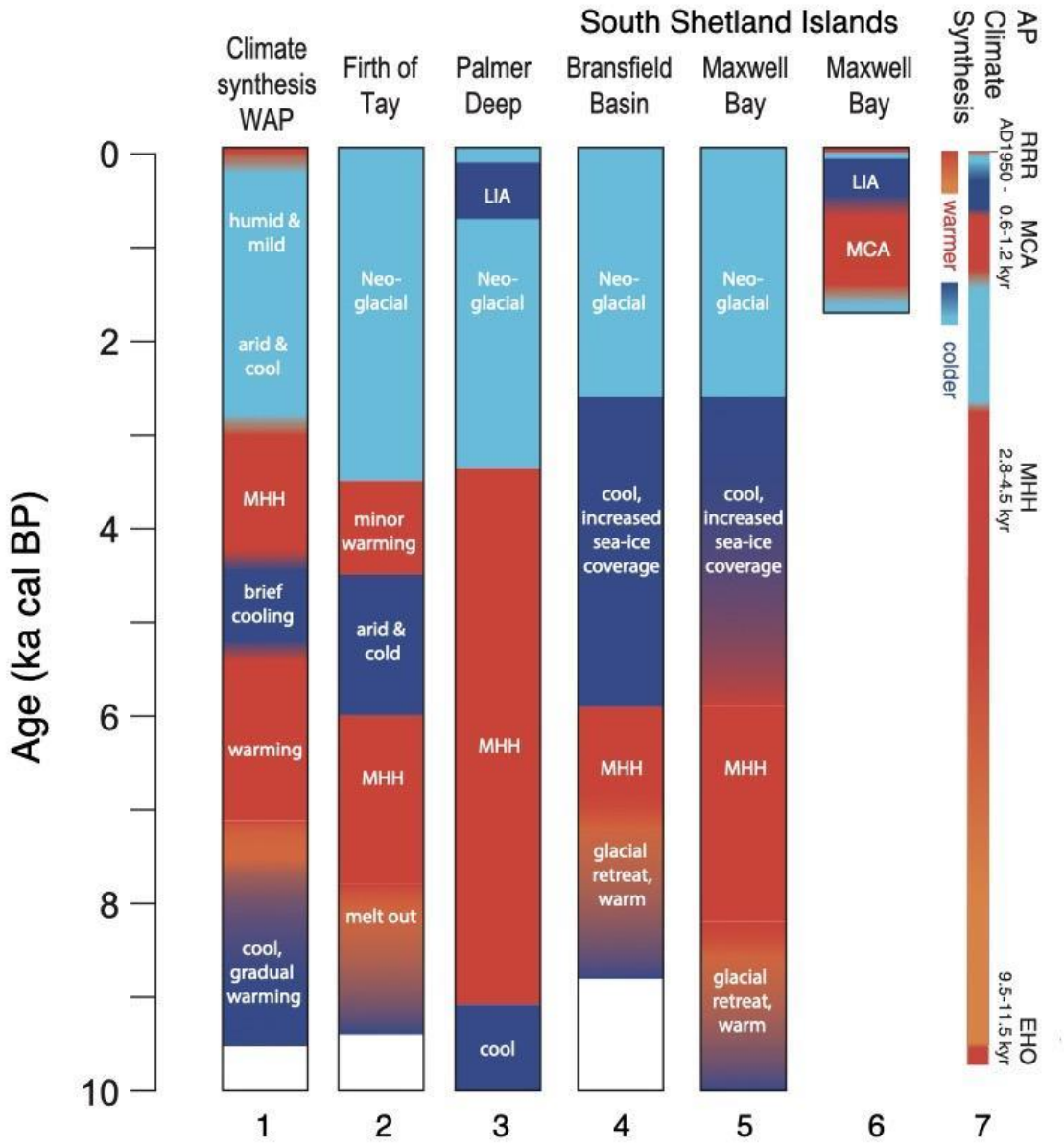

Figure S7. Palaeoclimate summary for the Antarctic Peninsula and the South Shetland Islands. 1-Ingólfsson et al., (2003); 2-Michalchuk et al. (2009); 3-Domack et al., (2001); 4-Heroy et al. (2008); 5-Milliken et al. (2009); 6-Monien et al. (2011) and Hass et al. (2010); 7-Bentley et al. (2009) where EHO = Early Holocene Climate Optimum, MHH = Mid Holocene Hypsithermal, MCA = Mediaeval Climate Anomaly; RRR = Recent Rapid Warming; LIA = Little Ice Age; AP = Antarctic Peninsula; WAP = Western Antarctic Peninsula.

Table S1. Results of textural analyses in samples from the new Pingfo II (nPII) section. Data are mass percentages.

Sample depth (m)	Altitude (m a.s.l.)	Facies	Gravel	Very Coarse Sand >1 mm	Coarse Sand >0.5 mm	Medium Sand >0.25 mm	Fine Sand >0.125 mm	Very Fine Sand >0,063 mm	Silt	Clay
0.35	5.65	6	22.5	9.4	9.1	10.5	11.2	5.0	18.5	13.8
1.05	4.9	5	14.5	17.4	18.2	21.4	19.5	4.3	3.6	1.2
1.35	4.65	5-4	0.2	0.6	2.2	26.5	61.1	5.5	1.4	2.5
1.5	4.5	4	0.2	0.1	0.4	16.4	65.0	11.3	2.7	3.9
1.65	4.35	4	2.0	0.5	1.8	14.5	54.8	16.4	7.5	2.5
1.85	4.15	4-3	0.0	0.1	0.5	25.0	66.2	5.3	2.2	0.7
1.9	4.1	3	3.2	1.0	2.1	10.5	47.9	19.2	13.6	2.5
2.17	3.83	3	1.8	0.5	0.7	4.2	44.8	27.8	14.7	5.5
2.37	3.63	3	0.4	0.1	0.2	2.1	48.5	35.4	10.6	2.8
2.62	3.38	3	5.9	0.5	0.7	3.8	39.2	30.2	15.9	3.8
2.87	3.13	3	0.4	0.1	0.3	1.2	31.9	42.1	20.9	3.0
2.97	3.03	1	0.1	0.2	0.8	4.7	56.7	28.1	8.2	1.2
3.15	2.85	1	0.4	0.3	1.1	5.8	57.7	20.6	12.3	1.9

Table S2. ^{210}Pb and ^{137}Cs data for Matias Lake (MAT1). Dated sampled: 19/11/2011.

Depth (cm)	Depth (mid) (cm)	Dry bulk density (g/cm^{-3})	^{210}Pb total (Bq g^{-1})	^{214}Bi supported ^{210}Pb (Bq g^{-1})	^{214}Pb supported ^{210}Pb (Bq g^{-1})	^{210}Pb unsupported ^{210}Pb (Bq g^{-1})	^{137}Cs (Bq g^{-1})	^{241}Am (Bq g^{-1})	CRS Age (years)	CRS age (Year CE)	Years before 2011 CE	±10 % error	Sediment velocity (cm J^{-1})	DMAR (g cm^{-1} J^{-1})
0-2	1.00	0.3704	0.055	-	0.018	0.037	0.011	0	14	1998	13	1	0.139	0.0516
2-2.5	2.25	0.3990	0.074	0.021	0.018	0.055	0.000	0	18	1994	17	2	0.131	0.0522
2.5-3	2.75	0.3753	0.047	-	0.018	0.029	0.004	0	23	1989	22	2	0.115	0.0432
3-3.5	3.25	0.3748	0.043	0.017	0.014	0.028	0.000	0	27	1985	26	3	0.105	0.0395
3.5-4	3.75	0.3736	0.039	0.019	0.019	0.020	0.012	0	31	1981	30	3	0.127	0.0474
4-4.5	4.25	0.3889	0.039	0.017	0.018	0.022	0.024	0	36	1976	35	4	0.098	0.0383
4.5-5	4.75	0.3617	0.033	0.015	0.015	0.018	0.036	0	41	1971	40	4	0.109	0.0392
5-5.5	5.25	0.3895	0.039	0.017	0.016	0.023	0.037	0	48	1964	47	5	0.067	0.0260
5.5-6	5.75	0.3792	0.028	-	0.018	0.010	0.021	0	52	1960	51	5	0.129	0.0489
6-6.5	6.25	0.3532	0.029	0.015	0.016	0.014	0.012	0	58	1954	57	6	0.088	0.0312
6.5-7	6.75	0.3731	0.032	0.016	0.015	0.017	0.004	0	67	1945	66	7	0.054	0.0202
7-7.5	7.25	0.3732	0.032	0.020	0.019	0.013	0.004	0	76	1935	76	8	0.053	0.0200
7.5-8	7.75	0.4103	0.028	0.016	0.015	0.013	0.000	0	91	1920	91	9	0.033	0.0137
8-8.5	8.25	0.3584	0.022	0.014	0.015	0.008	0.000	0	103	1908	103	10	0.042	0.0149
8.5-9	8.75	0.3562	0.026	0.016	0.015	0.011	0.000	0	136	1876	135	13	0.015	0.0055
9-9.5	9.25	0.3493	0.018	0.016	0.015	0.003	-	0	153	1859	152	15	0.030	0.0103
9.5-10	9.75	0.3114	0.022	0.017	0.019	0.004	-	0	-	-	-	-	-	-

Table S3. ^{210}Pb and ^{137}Cs data for Lake L15 (L15-H16). Date sampled: 29/11/2021

Depth (cm)	Depth (mid) (cm)	Dry bulk density (g/cm^{-3})	^{210}Pb total (Bq g^{-1})	^{214}Bi supported ^{210}Pb (Bq g^{-1})	^{214}Pb supported ^{210}Pb (Bq g^{-1})	^{210}Pb unsupported ^{210}Pb (Bq g^{-1})	^{137}Cs (Bq g^{-1})	^{241}Am (Bq g^{-1})	CRS Age (years)	CRS age (Year CE)	Sediment velocity (cm J^{-1})	DMAR (g cm^{-1} J^{-1})
0-1	0.50	0.67	0.091	0.012	0.012	0.074	0.041	0	10	2002	0.100	0.0667
1-2	1.50	0.66	0.095	0.012	0.013	0.077	0.024	0	26	1986	0.064	0.0426
2-3	2.50	0.64	0.086	0.012	0.012	0.069	0.021	0	50	1961	0.040	0.0257
3-4	3.50	0.63	0.067	0.012	0.013	0.050	0.019	0	112	1900	0.016	0.0102
4-4.5	4.25	0.52	0.029	0.011	0.011	0.016	0.014	0	162	1850	0.015	0.0079
5-5.5	5.25	0.47	0.02	0.014	0.014	0.005	0.009	0	-	-	-	-
5.5-6	5.75	0.46	0.015	0.013	0.013	0.001	0.009	0	-	-	-	-
6-6.5	6.25	0.45	0.018	0.013	0.015	0.003	0.002	0	-	-	-	-
6.5-7	6.75	0.42	0.009	0.014	0.014	-0.006	0.001	0	209	1803	-	-
7-7.5	7.25	0.39	0.016	0.0128	0.012	0.003	0.001	0	-	-	-	-
7.5-8	7.75	0.39	0.014	0.014	0.014	-0.001	0.011	0	-	-	-	-
8-8.5	8.25	0.39	0.017	0.015	0.014	0.001	0.008	0	-	-	-	-
8.5-9	8.75	0.36	0.017	0.013	0.013	0.003	0.000	0	-	-	-	-
9-9.5	9.25	0.35	0.0164	0.0148	0.014	0.001	0.000	0	-	-	-	-
9.5-10	9.75	0.34	0.02	0.013	0.015	0.005	0.000	0	-	-	-	-

Table S4. Differential GPS (dGPS) survey data for Lake L15 (GPS Lake).

Site		Day_of_year	Decimal_hour	Long.	Lat.	Ellipsoidal_height_m	Corrected_height_m
L15_OUT1	1962	331	18.82597222	-62.24046018	-58.67726735	42.43	20.95
L15_OUT2	1924	331	19.38430556	-62.24079061	-58.67702054	42.91	21.43
L15_OUT3	1921	331	19.93694445	-62.24093101	-58.67709091	42.55	21.07
L15 OUT4	2355	331	20.54888889	-62.24091399	-58.67772081	43.02	21.54
L15 IN1	1237	331	21.08888889	-62.24040484	-58.67823356	42.54	21.06
P5	1964	335	19.08069445	-62.24269298	-58.67656843	61.86	40.38
L15 IN_P3	1803	335	20.02444444	-62.24099213	-58.67781173	43.88	22.40

Table S5. Water chemistry data for Lake L5 (Matias Lake; 17/11/2011). Notes: the DO% sensor was run for 10-15 minutes to stabilise inside a sealed beaker with a damp sponge and Calibrated using atmospheric pressure of 1012.0 mbar (from Garmin barGPS); air temp ~1°C and stable temp./pressure during measurement.

Tape Depth (cm)	Pressure (P_{sia})	Probe depth (m)	Probe interval (cm)	Temp. (°C)	Specific conductivity ($mScm^{-3}$)	Conductivity ($mScm^{-1}$)	Salinity (ppt)	TDS (g/L)	DO (%)	DO Conc (mgL^{-1})	pH	pHmV	Res. (Ohm.cm)	Ice/water
20	14.736	0.187	-	1.35	0.096	0.053	0.04	0.063	55.1	7.70	6.17	10.9	18947.0	(Re)frozen snow/ice
20	14.742	0.192	0.005	1.25	0.094	0.051	0.04	0.061	71.9	10.15	6.35	1.9	19511.8	(Re)frozen snow/ice
30	14.866	0.279	0.087	0.96	0.093	0.051	0.04	0.061	65.3	9.29	6.46	-3.6	19796.0	(Re)frozen snow/ice
40	14.987	0.364	0.085	0.69	0.094	0.050	0.04	0.061	64.8	9.29	6.55	-8.1	19882.9	(Re)frozen snow/ice
50	15.097	0.441	0.077	0.71	0.093	0.050	0.04	0.061	52.9	7.58	6.62	-11.3	20015.7	(Re)frozen snow/ice
60	15.238	0.541	0.100	0.39	0.094	0.050	0.04	0.061	59.3	8.57	6.70	-15.5	20122.6	(Re)frozen snow/ice
70	15.326	0.603	0.062	0.40	0.093	0.049	0.04	0.060	65.2	9.42	6.80	-20.2	20265.3	(Re)frozen snow/ice
80	15.478	0.710	0.107	0.18	0.093	0.049	0.04	0.060	59.8	8.69	6.81	-21.0	20458.2	(Re)frozen snow/ice
90	15.593	0.791	0.081	0.20	0.093	0.049	0.04	0.060	57.5	8.35	6.89	-24.5	20498.6	(Re)frozen snow/ice
100	15.755	0.905	0.114	0.14	0.092	0.048	0.04	0.060	55.5	8.08	6.94	-27.1	20652.1	(Re)frozen snow/ice
110	15.861	0.979	0.074	0.14	0.092	0.049	0.04	0.060	43.0	6.26	6.92	-26.2	20600.8	(Re)frozen snow/ice
120	16.005	1.081	0.102	0.12	0.092	0.048	0.04	0.060	57.0	8.30	6.98	-29.3	20663.0	(Re)frozen snow/ice
130	16.138	1.175	0.094	0.10	0.092	0.048	0.04	0.060	60.3	8.79	6.99	-29.7	20703.9	Lake ice
140	16.286	1.279	0.104	0.09	0.092	0.048	0.04	0.060	56.8	8.29	7.01	-30.6	20778.3	Lake ice
150	16.434	1.383	0.104	0.08	0.092	0.048	0.04	0.060	52.2	7.61	7.03	-31.4	20787.0	Lake ice
160	16.557	1.470	0.087	0.08	0.092	0.048	0.04	0.060	54.3	7.92	7.04	-32.1	20832.9	Lake ice
170	16.711	1.578	0.108	0.06	0.092	0.048	0.04	0.060	55.0	8.02	7.04	-31.9	20858.8	Lake ice
180	16.826	1.659	0.081	0.06	0.091	0.048	0.04	0.059	49.0	7.15	7.02	-30.9	20878.5	Lake ice
190	16.962	1.755	0.096	0.33	0.090	0.048	0.04	0.058	72.3	10.47	7.04	-32.0	21033.4	Lake ice influenced
200	17.127	1.871	0.116	0.48	0.088	0.047	0.04	0.057	62.1	8.96	7.05	-32.4	21411.6	Lake ice influenced
210	17.253	1.960	0.089	0.57	0.085	0.045	0.04	0.055	56.4	8.12	7.04	-32.1	21983.3	Lake ice influenced
220	17.404	2.066	0.106	0.66	0.085	0.046	0.04	0.055	53.8	7.73	7.07	-33.3	21929.6	Lake ice influenced
230	17.527	2.153	0.087	0.71	0.086	0.046	0.04	0.056	50.8	7.28	7.01	-30.6	21604.3	Lake ice influenced
240	17.663	2.249	0.096	0.76	0.087	0.047	0.04	0.056	52.1	7.46	7.04	-31.8	21444.0	Lake ice influenced
250	17.827	2.364	0.115	0.82	0.087	0.047	0.04	0.057	34.7	4.95	7.03	-31.4	21260.6	Lake ice influenced
260	17.990	2.479	0.115	0.87	0.087	0.047	0.04	0.057	56.3	8.04	7.07	-33.5	21261.3	Lake ice influenced
270	18.100	2.557	0.078	0.91	0.087	0.047	0.04	0.057	54.2	7.72	7.03	-31.7	21235.0	Lake ice influenced
280	18.239	2.654	0.097	0.98	0.087	0.047	0.04	0.056	58.4	8.31	7.04	-31.8	21338.2	Lake ice influenced

290	18.394	2.764	0.110	1.02	0.086	0.047	0.04	0.056	60.9	8.65	7.03	-31.4	21362.1	Lake ice influenced
300	18.554	2.877	0.113	0.96	0.104	0.056	0.05	0.067	49.6	7.07	7.00	-30.1	17814.5	Water/ice free
310	18.692	2.973	0.096	0.93	0.129	0.070	0.06	0.084	44.4	6.32	7.03	-30.8	14324.7	Water/ice free
320	18.809	3.056	0.083	0.92	0.144	0.078	0.07	0.094	50.4	7.18	7.03	-31.6	12818.9	Water/ice free
330	18.950	3.155	0.099	0.91	0.160	0.086	0.07	0.104	48.9	6.97	7.03	-31.4	11605.0	Water/ice free
340	19.093	3.256	0.101	0.91	0.159	0.086	0.07	0.103	42.9	6.11	7.03	-31.7	11680.7	Water/ice free
350	19.263	3.375	0.119	0.91	0.161	0.087	0.08	0.105	44.4	6.32	7.03	-31.6	11472.2	Water/ice free
360	19.393	3.467	0.092	0.91	0.162	0.087	0.08	0.105	53.0	7.56	7.02	-30.8	11467.9	Water/ice free
370	19.549	3.577	0.110	0.91	0.161	0.087	0.08	0.105	44.2	6.30	7.00	-30.1	11483.7	Water/ice free
380	19.657	3.654	0.077	0.92	0.159	0.086	0.07	0.104	46.4	6.61	7.03	-31.3	11618.0	Water/ice free
390	19.823	3.770	0.116	0.92	0.161	0.087	0.08	0.105	42.6	6.07	7.00	-29.8	11512.0	Water/ice free
400	19.951	3.860	0.090	0.93	0.159	0.086	0.07	0.103	45.5	6.48	6.99	-29.7	11665.4	Water/ice free
410	20.111	3.973	0.113	0.94	0.160	0.087	0.07	0.104	45.4	6.46	6.97	-28.6	11554.9	Water/ice free
420	20.234	4.059	0.086	0.95	0.158	0.086	0.07	0.103	42.6	6.06	6.98	-29.1	11677.8	Water/ice free
430	20.381	4.163	0.104	0.96	0.160	0.087	0.07	0.104	43.4	6.17	6.91	-25.9	11548.3	Water/ice free
440	20.542	4.277	0.114	0.97	0.160	0.087	0.07	0.104	46.6	6.63	6.94	-26.9	11545.1	Water/ice free
450	20.685	4.377	0.100	0.98	0.160	0.087	0.07	0.104	42.1	5.98	6.90	-25.2	11526.0	Water/ice free
460	20.831	4.480	0.103	0.98	0.161	0.087	0.08	0.104	43.1	6.13	6.90	-25.4	11498.9	Water/ice free
470	20.971	4.578	0.098	0.99	0.161	0.087	0.08	0.105	41.8	5.95	6.87	-23.6	11471.7	Water/ice free
480	21.241	4.769	0.191	0.99	0.162	0.088	0.08	0.105	32.0	4.55	6.84	-22.4	11420.3	Water/ice free
490	21.421	4.896	0.127	0.99	0.164	0.089	0.08	0.107	43.1	6.12	6.74	-17.3	11250.9	Water/ice free
500	21.547	4.984	0.088	1.00	0.165	0.090	0.08	0.108	36.5	5.19	6.74	-17.2	11164.3	Water/ice free
510	21.660	5.064	0.080	1.00	0.166	0.090	0.08	0.108	30.3	4.30	6.67	-13.9	11133.7	Water/ice free
520	21.815	5.173	0.109	1.01	0.165	0.090	0.08	0.107	31.6	4.49	6.65	-12.8	11160.7	Water/ice free
530	21.941	5.262	0.089	1.03	0.166	0.090	0.08	0.108	31.8	4.51	6.58	-9.5	11125.4	Water/ice free
540	22.095	5.370	0.108	1.04	0.166	0.090	0.08	0.108	28.0	3.97	6.55	-8.0	11116.3	Water/ice free
550	22.203	5.447	0.077	1.05	0.166	0.090	0.08	0.108	27.2	3.86	6.52	-6.6	11106.0	Water/ice free
560	22.241	5.473	0.026	1.06	0.165	0.089	0.08	0.107	25.5	3.61	6.52	-6.4	11189.1	Sediment/water
570	22.289	5.507	0.034	1.06	0.166	0.090	0.08	0.108	27.1	3.84	6.47	-3.9	11080.3	Sediment
580	22.322	5.530	0.023	1.06	0.165	0.089	0.08	0.107	27.2	3.86	6.47	-4.1	11187.7	Sediment
590	22.357	5.555	0.025	1.06	0.166	0.090	0.08	0.108	27.0	3.83	6.44	-2.7	11076.2	Sediment
-	21.053	4.636	0.091	0.99	0.163	0.088	0.077	0.106	37.7	5.36	6.78	-19.2	11357.5	Mean
-	0.999	0.704	0.037	0.05	0.003	0.002	0.005	0.002	8.28	1.19	0.21	10.2	210.5	SD

Table S6. Water chemistry data for Lake L15 (GPS Lake; 17/11/2011). Notes: the DO% sensor was run for 10-15 minutes to stabilise inside sealed beaker with damp sponge and Calibrated using atmospheric pressure of 979.4 mbar (from Garmin barGPS); air temp. ~1°C with stable temp./pressure during measurement.

Tape Depth (cm)	Pressure (P_{sia})	Probe depth (m)	Probe interval (cm)	Temp. (°C)	Specific conductivity ($mScm^{-3}$)	Conductivity ($mScm^{-1}$)	Salinity (ppt)	TDS (g/L)	DO (%)	DO Conc (mgL^{-1})	pH	pHmV	Res. (Ohm.cm)	Ice/water
20	14.514	0.34		0.24	0.088	0.046	0.04	0.057	92.7	13.46	6.40	-0.9	21602.8	(Re)frozen snow/ice
20	14.472	0.31	-0.030	0.24	0.090	0.047	0.04	0.058	67.2	9.76	6.39	0.0	21134.9	(Re)frozen snow/ice
20	14.478	0.31	0.005	0.20	0.089	0.047	0.04	0.058	62.3	9.06	6.30	4.1	21293.6	(Re)frozen snow/ice
30	14.600	0.40	0.086	0.16	0.089	0.047	0.04	0.058	67.0	9.74	6.27	5.6	21340.3	(Re)frozen snow/ice
40	14.726	0.49	0.088	0.14	0.089	0.047	0.04	0.058	61.4	8.94	6.23	7.4	21426.4	(Re)frozen snow/ice
50	14.871	0.59	0.103	0.12	0.089	0.047	0.04	0.058	63.3	9.22	6.20	9.0	21438.9	(Re)frozen snow/ice
60	14.990	0.67	0.083	0.13	0.089	0.047	0.04	0.058	62.3	9.08	6.19	9.5	21443.6	(Re)frozen snow/ice
70	15.116	0.67	-0.001	0.12	0.089	0.047	0.04	0.058	64.8	9.44	6.17	10.6	21474.1	(Re)frozen snow/ice
80	15.253	0.76	0.090	0.12	0.089	0.047	0.04	0.058	33.6	4.90	6.14	11.8	21462.6	Lake ice
90	15.415	0.86	0.097	0.13	0.088	0.046	0.04	0.057	46.5	6.77	6.13	12.4	21568.6	Lake ice
100	15.544	0.97	0.114	0.15	0.088	0.046	0.04	0.057	52.1	7.58	6.15	11.4	21554.6	Lake ice
110	15.681	1.06	0.091	0.18	0.088	0.046	0.04	0.057	53.0	7.71	6.14	11.9	21537.8	Water/ice free
120	15.798	1.24	0.179	0.64	0.087	0.046	0.04	0.056	46.6	6.68	6.11	13.4	21612.9	Water/ice free
130	15.932	1.34	0.094	0.88	0.086	0.046	0.04	0.056	70.2	10.01	6.08	15.2	21514.5	Water/ice free
140	16.083	1.44	0.107	1.00	0.086	0.047	0.04	0.056	53.2	7.61	6.10	13.9	21424.4	Water/ice free
150	16.235	1.55	0.107	1.04	0.086	0.047	0.04	0.056	56.8	8.06	6.10	14.2	21331.8	Water/ice free
160	16.372	1.65	0.096	1.13	0.086	0.047	0.04	0.056	53.3	7.55	6.09	14.8	21332.1	Water/ice free
170	16.503	1.74	0.092	1.19	0.086	0.047	0.04	0.056	54.6	7.73	6.07	15.7	21204.5	Water/ice free
180	16.647	1.84	0.102	1.27	0.089	0.048	0.04	0.058	48.1	6.78	6.04	17.1	20625.7	Water/ice free
190	16.764	1.92	0.082	1.31	0.089	0.049	0.04	0.058	58.2	8.21	5.99	19.4	20591.0	Water/ice free
200	16.939	2.05	0.124	1.35	0.098	0.054	0.05	0.064	49.6	6.98	5.97	20.3	18556.5	Water/ice free
210	17.060	2.13	0.084	1.24	0.115	0.063	0.05	0.075	38.3	5.41	5.93	22.2	15880.0	Sediment/water
212	17.095	2.16	0.025	1.23	0.121	0.066	0.06	0.079	36.5	5.15	5.93	22.5	15133.7	Sediment
-	15.699	1.15	0.083	0.62	0.091	0.049	0.04	0.059	56.2	8.08	6.14	12.2	20716.75	Mean
-	0.888	0.63	0.046	0.51	0.009	0.005	0.00	0.006	12.7	1.88	0.13	6.2	1766.6	SD

Table S7. Comparison of individual and weighted mean Marine13 and Marine20 DR data for the Antarctic Peninsula and Signy Island region in the CALIB online database (http://calib.org/marine/)

A

Curve	Map No.	Lon	Lat	ΔR (^{14}C yrs)	ΔR Err	Reference	Locality	Collection Year	Res. Age	Res. Err.	C14 age	C14 err.	Lab ID	Genus	Species	Dist. (km)
Marine13	523	-56.98	-63.4	829	50	Bjorck, S, :1991	Hope Bay, NE Ant. Pen.	1903	1160	51	1280	50	Lu-3101			166
Marine13	522	-67.28	-67.87	956	40	Berkman, P :1996	S Ant Pen: 25-30 m depth	1940	1267	41	1416	40	GX-18582	*Adamussium*	*colbecki*	744
Marine13	521	-67.00	-68.65	1016	39	Berkman, P :1996	S Ant Pen: 25-30 m depth	1940	1327	40	1476	39	GX-18581	*Adamussium*	*colbecki*	810
Marine13	516	-45.63	-61.72	831	50	Peck, L S, :1996	Signy Island, Antarctica	1953	1123	52	1300	50	AA-16912	*Liothyrella*	*uva*	692
Marine13	517	-45.63	-61.72	701	45	Peck, L S, :1996	Signy Island, Antarctica	1950	1009	47	1170	45	AA-16913	*Liothyrella*	*uva*	692
Marine13	518	-45.63	-61.72	872	45	Peck, L S, :1996	Signy Island, Antarctica	1949	1181	47	1340	45	AA-16917	*Liothyrella*	*uva*	692
Marine13	368	-72.65	-51.7	221	40	Ingram, B L :1996	Puerto Natales, Chile	1939	530	41	680	40	CAMS-17918	*Mytilus*	*californianaus*	1428
Marine13	1081	-62.07	-38.92	143	40	Gomez, et al:2008	Parejas Creek	1935	442	41	600	40	BETA-216775	*Littoridina*	*australis*	2596
Marine13	1079	-62.1	-38.9	-229	40	Gomez, et al:2008	Belgrano Port	1920	91	41	220	40	BETA-216782	*Pitar*	*rostratus*	2598
Marine13	1080	-62.1	-38.9	41	40	Gomez, et al:2008	Belgrano Port	1920	356	41	490	40	BETA-223397	*Pitar*	*rostratus*	2598
Marine20	523	-56.98	-63.4	669	50	Bjorck, S, :1991	Hope Bay, NE Ant. Pen.	1903	1184	51	1280	50	Lu-3101		*sp.*	166
Marine20	522	-67.28	-67.87	813	40	Berkman, P :1996	S Ant Pen: 25-30 m depth	1940	1246	41	1416	40	GX-18582	*Adamussium*	*colbecki*	744
Marine20	521	-67	-68.65	873	39	Berkman, P :1996	S Ant Pen: 25-30 m depth	1940	1306	40	1476	39	GX-18581	*Adamussium*	*colbecki*	810
Marine20	516	-45.63	-61.72	697	50	Peck, L S, :1996	Signy Island, Antarctica	1953	1095	52	1300	50	AA-16912	*Liothyrella*	*uva*	692
Marine20	517	-45.63	-61.72	567	45	Peck, L S, :1996	Signy Island, Antarctica	1950	971	47	1170	45	AA-16913	*Liothyrella*	*uva*	692
Marine20	518	-45.63	-61.72	737	45	Peck, L S, :1996	Signy Island, Antarctica	1949	1143	47	1340	45	AA-16917	*Liothyrella*	*uva*	692
Marine20	2020	-69.5	-54.317	-73	60	Merino-Campos et al (2019)	Seno Almirantazgo	1955	347	26	530	20	UCIAMS-134087	*Nacella*	*deaurata*	1071
Marine20	2022	-70.433	-54.433	-73	60	Merino-Campos et al (2019)	Seno Agostini	1954	348	25	530	20	UCIAMS-134088	*Nacella*	*magellanica*	1092
Marine20	2021	-70.4507	-53.2912	-108	60	Merino-Campos et al (2019)	Punta Chilota	1953	315	25	495	20	UCIAMS-134083	*Nacella*	*nica*	1200
Marine20	2013	-70.9559	-53.6127	-98	60	Merino-Campos et al (2019)	Bulnes Fort, Magallanes	1954	323	25	505	20	UCIAMS-134084	*Fisurella*	*cumingi*	1187

Notes: 10 nearest datapoints to SSI (-62.18104, -58.86096)

Table S7 contd.

B

	Marine13: Regional Combinatons	ΔR (WM)	ΔR (SD)	Reference	n	Map No.
1	All Antarctic Peninsula and Signy	881	115	Bjorck, S, :1991; Berkman, P :1996; Peck, L S, :1996	6	516, 517, 518, 521, 522, 523
2	All Antarctic Peninsula	949	88	Bjorck, S, :1991; Berkman, P :1996	3	521, 522, 523
3	Southern Antarctic Peninsula	987	42	Berkman, P A:1996	2	521, 522
4	NE Antarctic Peninsula and Signy	806	78	Bjorck, S, :1991; Peck, L S, :1996	4	516, 517, 518, 523
5	Signy	799	92	Peck, L S, :1996	3	516, 517, 518
-	NE Antarctic Peninsula	829	50	Bjorck, S, :1991	1	523

	Marine20: Regional Combinatons	ΔR (WM)	ΔR (Uncert.)	Reference	n	Map No.	Mar20-Mar13
1	All Antarctic Peninsula and Signy	740	113	Bjorck, S, :1991; Berkman, P :1996; Peck, L S, :1996	6	516, 517, 518, 521, 522, 523	-141
2	All Antarctic Peninsula	802	97	Bjorck, S, :1991; Berkman, P :1996	3	521, 522, 523	-147
3	Southern Antarctic Peninsula	844	42	Berkman, P A:1996	2	521, 522	-143
4	NE Antarctic Peninsula and Signy	666	76	Bjorck, S, :1991; Peck, L S, :1996	4	516, 517, 518, 523	-140
5	Signy	665	91	Peck, L S, :1996	3	516, 517, 518	-134
-	NE Antarctic Peninsula	669	50	Bjorck, S, :1991	1	523	-160

7. References

Appleby, PG, and Oldfield F. (1978). "The calculation of lead-210 dates assuming a constant rate of supply of unsupported ^{210}Pb to the sediment." *Catena* 5(1): 1-8.

Bard E, Tuna T, Fagault Y, et al. (2015) AixMICADAS, the accelerator mass spectrometer dedicated to 14C recently installed in Aix-en-Provence, France. *Nuclear Instruments and Methods in Physics Research Section B: Beam Interactions with Materials and Atoms* 361: 80-86.

Bentley MJ, Hodgson DA, Smith JA, et al. (2009) Mechanisms of Holocene palaeoenvironmental change in the Antarctic Peninsula region. *The Holocene* 19: 51-69.

Berkman PA and Forman SL. (1996) Pre-bomb radiocarbon and the reservoir correction for calcareous marine species in the Southern Ocean. *Geophysical Research Letters* 23: 363-366.

Björck S, Hjort, C, Ingolfsson O, Skog G. (1991) Radiocarbon dates from the Antarctic Peninsula region — problems and potential. In: Lowe JJ (ed) Radiocarbon dating: recent applications and future potential. *Quaternary Proceedings* 55–65.

Blard PH and Farley KA. (2008) The influence of radiogenic ^{4}He on cosmogenic ^{3}He determinations in volcanic olivine and pyroxene. *Earth and Planetary Science Letters* 276: 20-29.

Blard PH, Balco G, Burnard PG, et al. (2015) An inter-laboratory comparison of cosmogenic ^{3}He and radiogenic ^{4}He in the CRONUS-P pyroxene standard. *Quaternary Geochronology* 26: 11-19.

Curl JE. (1980) A glacial history of the South Shetland Islands, Antarctica. Institute of Polar Studies Report No. 63. The Ohio State University, 129.

del Valle RA, Tatur A, Lusky J, et al. (2004) Cambios morfológicos recientes en lagos de la península Potter, isla 25 de Mayo, islas Shetland del Sur, Antártida. *Revista de la Asociación Geológica Argentina* 59: 443-450.

Domack EW and Ishman SE. (1992) Magnetic susceptibility of Antarctic glacial marine sediments. *Antarctic Journal of the United States* 27: 64-65.

Domack E, Leventer A, Dunbar R, et al. (2001) Chronology of the Palmer Deep site, Antarctic Peninsula: a Holocene palaeoenvironmental reference for the circum-Antarctic. *The Holocene* 11: 1-9.

Dunai TJ, Stuart FM, Pik R, et al. (2007) Production of ^{3}He in crustal rocks by cosmogenic thermal neutrons. *Earth and Planetary Science Letters* 258: 228-236.

Emslie SD. (1995) Age and taphonomy of abandoned penguin rookeries in the Antarctic Peninsula region. Polar Record 31: 409-418.

Emslie SD. (2001) Radiocarbon dates from abandoned penguin colonies in the Antarctic Peninsula region. *Antarctic Science* 13: 289-295.

Emslie SD, Polito MJ and Patterson WP. (2013) Stable isotope analysis of ancient and modern gentoo penguin egg membrane and the krill surplus hypothesis in Antarctica. *Antarctic Science* 25: 213-218.

Emslie SD, Romero M, Juáres MA and Argota MR. (2019) Holocene occupation history of pygoscelid penguins at Stranger Point, King George (25 de Mayo) Island, northern Antarctic Peninsula. *The Holocene*: 0959683619875814.

Falk U and Sala H. (2015) Winter melt conditions of the inland ice cap on King George Island, Antarctic Peninsula. *Erdkunde* 69: 341-363.

Gordon JE and Harkness DD. (1992) Magnitude and geographic variation of the radiocarbon content in Antarctic marine life: Implications for reservoir corrections in radiocarbon dating. *Quaternary Science Reviews* 11: 697-708.

Hall BL. (2010) Holocene relative sea-level changes and ice fluctuations in the South Shetland Islands. *Global and Planetary Change* 74: 15-26.

Hall BL, Henderson GM, Baroni C and Kellogg TB. (2010) Constant Holocene Southern-Ocean 14C reservoir ages and ice-shelf flow rates. Earth and Planetary Science Letters 296: 115-123.

Hass HC, Kuhn G, Monien P, et al. (2010) Climate fluctuations during the past two millennia as recorded in sediments from Maxwell Bay, South Shetland Islands, West Antarctica. *Geological Society, London, Special Publications* 344: 243-260.

Heaton TJ, Köhler P, Butzin M, et al. (2020) Marine20—The Marine Radiocarbon Age Calibration Curve (0–55,000 cal BP). *Radiocarbon* 62: 779-820.

Heaton, TJ, Bard, E, Bronk Ramsey, C, et al. (2022). A response to community questions on the Marine20 radiocarbon age calibration curve: marine reservoir ages and the calibration of 14C samples from the oceans. Radiocarbon: 1-27. doi:10.1017/RDC.2022.66

Heroy DC, Sjunneskog C and Anderson JB. (2008) Holocene climate change in the Bransfield Basin, Antarctic Peninsula: evidence from sediment and diatom analysis. *Antarctic Science* 20: 69-87.

Hogg AG, Hua Q, Blackwell PG, et al. (2013) SHCal13 Southern Hemisphere Calibration, 0–50,000 Years cal BP. Radiocarbon 55: 1889-1903.

Hogg AG, Heaton TJ, Hua Q, et al. (2020) SHCal20 Southern Hemisphere Calibration, 0–55,000 Years cal BP. *Radiocarbon* 62: 759-778.

Ingólfsson Ó, Hjort C and Humlum O. (2003) Glacial and Climate History of the Antarctic Peninsula since the Last Glacial Maximum. *Arctic, Antarctic, and Alpine Research* 35: 175-186.

Michalchuk BR, Anderson JB, Wellner JS, et al. (2009) Holocene climate and glacial history of the northeastern Antarctic Peninsula: the marine sedimentary record from a long SHALDRIL core. *Quaternary Science Reviews* 28: 3049-3065.

Milliken KT, Anderson JB, Wellner JS, et al. (2009) High-resolution Holocene climate record from Maxwell Bay, South Shetland Islands, Antarctica. *Geol. Society of America Bulletin* 121: 1711-1725.

Monien P, Schnetger B, Brumsack H-J, et al. (2011) A geochemical record of late Holocene palaeoenvironmental changes at King George Island. *Antarctic Science* 23: 255-267.

Niedermann S, Bach W and Erzinger J. (1997) Noble gas evidence for a lower mantle component in MORBs from the southern East Pacific Rise: Decoupling of helium and neon isotope systematics. *Geochimica et Cosmochimica Acta* 61: 2697-2715.

Niedermann S. (2002) Cosmic-Ray-Produced Noble Gases in Terrestrial Rocks: Dating Tools for Surface Processes. *Reviews in Mineralogy and Geochemistry* 47: 731-784.

Ó Cofaigh C, Davies BJ, Livingstone SJ, et al. (2014) Reconstruction of ice-sheet changes in the Antarctic Peninsula since the Last Glacial Maximum. *Quaternary Science Reviews* 100: 87-110.

Protin M, Blard P-H, Marrocchi Y, et al. (2016) Irreversible adsorption of atmospheric helium on olivine: A lobster pot analogy. *Geochimica et Cosmochimica Acta* 179: 76-88.

Reimer PJ, Bard E, Bayliss A, et al. (2013) IntCal13 and Marine13 Radiocarbon Age Calibration Curves 0–50,000 Years cal BP. Radiocarbon 55: 1869-1887.

Roberts SJ, Monien P, Foster LC, et al. (2017) Past penguin colony responses to explosive volcanism on the Antarctic Peninsula. *Nature Communications* 8: 14914.

Simms AR, Ivins ER, DeWitt R, et al. (2012) Timing of the most recent Neoglacial advance and retreat in the South Shetland Islands, Antarctic Peninsula: insights from raised beaches and Holocene uplift rates. *Quaternary Science Reviews* 47: 41-55.

Simms AR, Bentley MJ, Simkins LM, et al. (2021) Evidence for a "Little Ice Age" glacial advance within the Antarctic Peninsula – Examples from glacially-overrun raised beaches. Quaternary Science Reviews 271: 107195.

Wacker L, Lippold J, Molnár M, et al. (2013) Towards radiocarbon dating of single foraminifera with a gas ion source. *Nuclear Instruments and Methods in Physics Research Section B: Beam Interactions with Materials and Atoms* 294: 307-310.

Watcham EP, Bentley MJ, Hodgson DA, et al. (2011) A new Holocene relative sea level curve for the South Shetland Islands, Antarctica. *Quaternary Science Reviews* 30: 3152-3170.

Williams AJ, Stuart FM, Day SJ, et al. (2005) Using pyroxene microphenocrysts to determine cosmogenic ^{3}He concentrations in old volcanic rocks: an example of landscape development in central Gran Canaria. *Quaternary Science Reviews* 24: 211-222.

Winkler JB. (2000) The role of snow cover on the cryptogamic vegetation in the maritime Antarctic (Potter Peninsula, King George Island). Bremerhaven: Alfred Wegener Institute for Polar and Marine Research. 10013/epic.10375.

Wunderle S, Saurer H and Grossmann H. (1998) Meteorological Conditions and Snow Cover Dymanics on the Potter Peninsula, King George Island, Antarctica. Das Künstenökosystem der Potter Cove, Antarktis. Eine Synopsis der Forschungsarbeiten im Rahmen der argentinisch-deutschen Kooperation in Dallmann Labour und an der Jubany–Station (1991-1997). *Berichte zur Polarforschung* 299: 15-27.